Evaluation of advanced phosphorus removal from slaughterhouse wastewater using industrial waste-based adsorbents

Shengdan Sun, Chuanping Feng, Shuang Tong, Yan Zhao, Nan Chen and Ming Zhu

ABSTRACT

Slaughterhouse wastewater (SWW) contains high concentrations of phosphorus (P) and is considered as a principal industrial contaminant that causes eutrophication. This study developed two kinds of economical P removal adsorbents using flue gas desulfurization gypsum (FGDG) as the main raw material and bentonite, clay, steel slag and fly ash as the additives. The maximum adsorption capacity of the adsorbent composed of 60% FGDG, 20% steel slag, and 20% fly ash (DSGA2) was found to be 15.85 mg P/g, which was 19 times that of the adsorbent synthesized using 60% FGDG, 30% bentonite, and 10% clay (DSGA1) (0.82 mg P/g). Surface adsorption, internal diffusion, and ionic dissolution co-existed in the P removal process. The adsorption capacity of DSGA2 (2.50 mg P/g) was also evaluated in column experiments. The removal efficiency was determined to be higher than 92% in the first 5 days, while the corresponding effluent concentration was lower than the Chinese upcoming SWW discharge limit of 2 mg P/L. Compared with DSGA1, DSGA2 (synthesized from various industrial wastes) showed obvious advantages in improving adsorption capacity of P. The results showed that DSGA2 is a promising adsorbent for the advanced removal of P from SWW in practical applications.

Key words | adsorption, chemical precipitation, industrial wastes, phosphorus removal, slaughterhouse wastewater

Shengdan Sun
Chuanping Feng
Nan Chen
School of Water Resources and Environment, MOE Key Laboratory of Groundwater Circulation and Environmental Evolution,
China University of Geosciences (Beijing),
Beijing, 100083,
China

Shengdan Sun
Shuang Tong (corresponding author)
Yan Zhao
Ming Zhu
Beijing Key Laboratory of Meat Processing Technology,
China Meat Research Center,
Beijing 100068,
China
E-mail: *selina_wen@foxmail.com*

HIGHLIGHTS

- We developed an efficient granular adsorbent based on industrial waste.
- P removal from slaughterhouse wastewater was achieved with reused industrial waste.
- Actual treated slaughterhouse wastewater was used in continuous flow experiments.
- Surface adsorption, internal diffusion and ionic dissolution played a role in the P removal process.

INTRODUCTION

Increased income and living standards have promoted the development of the slaughtering and meat processing industry over the last few decades (Bouwman *et al.* 2013). Effluent wastewater coming from slaughterhouse

wastewaters (SWW) contained 1,700–2,100 mg/L chemical oxygen demand (COD), 115–211 mg/L total nitrogen (TN) and 18.0–37.5 mg/L total phosphorus (TP) (Tong *et al.* 2019). It is obvious that large amounts of SWW discharged into the aquatic environments would lead to the eutrophication of surface water and pollution of groundwater.

Nowadays, the removal of phosphorus (P) from SWW is achieved using physicochemical (Prazeres *et al.* 2019) and

biological methods (Tong *et al.* 2019). Although biological methods, such as anaerobic and aerobic processes, are effective, strict operating conditions (Tong *et al.* 2019), high energy consumption and instable operations have limited their application in practical engineering. At the same time, the method of chemical precipitation is expensive (Prazeres *et al.* 2019). The method of adsorption has been widely used to treat SWW due to its high efficiency, and economical, and stable operation (Prazeres *et al.* 2019). In addition, due to the high selectivity of the adsorption method, the recovery of P was feasible (Nguyen *et al.* 2014). However, only a handful of studies has shown the removal of P from SWW using adsorption. Therefore, it is necessary to develop and study an efficient, stable, and economic adsorbent for the advanced removal of P from SWW to minimize the risk of contamination.

In order to save disposal costs and attain the goal of treating waste using wastes, there is an increasing trend of using industrial wastes to mitigate environmental pollution. Desulfurization gypsum (Chen *et al.* 2016), steel slag (Barca *et al.* 2014), and fly ash (Li *et al.* 2017) have been extensively studied as the P adsorbent due to their abundant calcium, iron, magnesium, and aluminum element content. The above studies have shown a low utilization efficiency and adsorption capacity of P. Some progress has been made in the preparation of composite adsorbents by modifying industrial materials, such as through the nano-modification (Chen *et al.* 2016) and acidic treatment of industrial wastes (Xue *et al.* 2009). Previous studies have confirmed that the adsorbents synthesized using industrial wastes are feasible for P removal from synthetic wastewater with only a single contaminant (Yin *et al.* 2020). However, the characteristics of SWW was much more complex than synthetic wastewater. Therefore, the adsorbents based on industrial wastes were evaluated for advanced P removal from SWW.

The main composition of flue gas desulfurization gypsum (FGDG) is the same as that of natural gypsum. It had been widely studied because no heavy metals dissolve out during the P removal process (Cheng *et al.* 2018). Therefore, in this study, FGDG was used as the main component to study the difference of performance between FGDG + natural crystal materials (bentonite and clay) and FGDG + industrial waste (steel slug and fly ash) for removing P from SWW. The particular objectives of the current work were to: (1) develop two different types of granulated adsorbents, which were based upon industrial wastes, and used to achieve advanced P removal from SWW, (2) investigate the maximum adsorption capacity and analyze the adsorption mechanisms of P, and (3) evaluate the influence of co-existing ions and the performance of practical wastewater treatment through packed column study. The results are expected to provide support for practical engineering application of such novel waste-based P-removing adsorbents.

MATERIALS AND METHODS

Experimental solution

1 L stock solution of 500 mg P/L was prepared by dissolving 2.1935 g KH_2PO_4 (anhydrous, analytical grade, China) in deionized water and diluted 20 times to 25 mg P/L before the experiments. After anaerobic and aerobic treatment of SWW, the effluent quality became better (with much lower COD and N species concentrations) but still contained high P. Hence, the actual secondary biological effluent of SWW was obtained from the laboratory-scale anaerobic and aerobic processes for tertiary P removal. Various characteristics of the SWW are presented in Table 1.

Preparation of DSGA1 and DSGA2

Several batches of adsorbents under different mixing ratios, particle size and calcination temperatures were made. After the test of P removal efficiency, two of them were selected for this study. DSGA1 (particle size of 2–5 mm) was composed of 60% FGDG, 30% bentonite, and 10% clay. The synthesized DSGA1 samples were calcined in a muffle furnace at 1,050 °C for 2 h. Conversely, DSGA2 (particle size of 2–5 mm) was composed of 60% FGDG, 20% steel slag, and 20% fly ash. The synthesized DSGA2 samples were calcined in a muffle furnace at 1,100 °C for 2 h.

FGDG used for this study was supplied by the Tangshan Sanyou Chemical Industry Co., Ltd, China. The clay was knar clay obtained from Tangshan Hebei, China. Bentonite was purchased from Sinopharm Chemical Reagent Co., Ltd,

Table 1 | Characteristics of the actual secondary effluent of SWW

Parameter (mg/L)	TN	NO_3^--N	NO_2^--N	TP	PO_4^{3-}-P	COD_{Cr}	pH
SWW	62.15	57.95	0.08	25.03	24.68	80.00	7.0–8.0

China. Steel slag and fly ash were obtained from Tangshan Jidong Cement Co., Ltd, China.

Before and after the experiments, both the adsorbents were analyzed using electron probe microanalysis (EPMA) (EPMA-1600, Shimadzu, Japan) to elemental analysis, X-ray diffraction (XRD) (Burker D8 focus, Germany) to crystallization phase analysis, and scanning electron microscopy (SEM) (SSX-550, Shimadzu, Japan) to study their surface characteristics. Specific area, porosity, and pore size distribution were obtained using the Brunauer–Emmett–Teller (BET) method (AUTOS-ORBiQ2, Quantachrome, USA) to study the corresponding total pore volume and average pore diameter.

Batch experiments

At room temperature $25 \pm 2\,°C$, 0.5 g DSGA1 and 0.5 g DSGA2 were separately placed in 500 mL conical flasks that contained 400 mL KH_2PO_4 solution (25 mg P/L). Duplicate conical flasks were made for each condition, and samples were taken in parallel. Flasks were all sealed and then placed into a constant temperature oscillator to shake at 60 r/min. Then, a 3 mL liquid sample was taken from each flask at 1, 2, 4, 8, 12, 18, and 24 h during the first day, followed by sampling after every 24 h until equilibrium.

The adsorption capacity of P for the two adsorbents was calculated using Equation (1):

$$Q_t = \frac{(C_0 - C_t)V}{M} \qquad (1)$$

where Q_t (mg P/g) is the adsorption capacity at time t, C_0 and C_t (mg P/L) are the initial concentration of P and the concentration of P at time t, respectively, V (L) is the volume at the measuring time of the solution, and M (g) is the mass of the adsorbent.

Continuous-flow experiments

In batch experiments, it was observed that DSGA2 had a larger capacity than DSGA1. Therefore, DSGA2 was chosen for further column experiments. The up-flow columns were made of polymethyl methacrylate with an internal diameter of 2.5 cm and length of 20.0 cm. The effective volume of the column was approximately 100 mL and was filled with about 53 g of DSGA2 to run at room temperature $(25 \pm 2\,°C)$. The influent was pumped into the bottom and overflowed from the top of the columns.

The equilibrium time was 360 h. obtained in a batch experiment. This was equivalent to 0.36 h in a column experiment (HRT). Considering the influence of contact time on the mass transfer process in the column study, safety factor 2 was introduced. The flow rate and the hydraulic retention time in the column study were 0.8 mL/min and 0.67 h, respectively. The influent for Column 1# was the actual SWW, coming from the secondary biological process, at a flow rate of 0.8 mL/min. The influent for Column 2# was the synthetic 25 mg P/L wastewater flowing at the same flow as Column 1#. When the effluent P concentration reached 10% of influent, the columns reached the breakthrough point. Similarly, 90% was the depletion point. Samples were taken four times a day before the columns reached the breakthrough point and then two times until they reached the depletion point. Given the effects of the co-existing anions in SWW on ions dissolution of DSGA2, the concentrations of NH_4^+, Na^+, Mg^{2+}, K^+, Ca^{2+}, Cl^-, NO_2^-, NO_3^-, and SO_4^{2-} were detected.

The maximum adsorption capacity obtained in batch experiments is usually greater than that in practical applications. Therefore, in this study, the adsorption capacity (Q_p) was calculated in experiments to provide a reference value for actual engineering design. Here, Q_p (mg P/g) was the adsorption capacity at the breakthrough point in columnar experiments. However, to obtain the effluent P concentration lower than the SWW discharge limit of 2 mg/L, the effluent concentration should be less than the 8% of the influent concentration, which means that the removal efficiency should be higher than 92%. Therefore, the adsorption capacity can be roughly calculated using Equation (2):

$$Q_p = \frac{(C_{in} - 2)Tv}{1000M} \qquad (2)$$

where C_{in} (mg/L) is the influent concentration, which has a maximum value when the influent concentration is unstable, T (min) is the total operation time of the column, its effluent P concentration exceeded the acceptable value of 2 mg P/L (discharge limit for SWW). v (mL/min) is the flow rate (0.8 mL/min). M (g) carries the same meanings as previously defined.
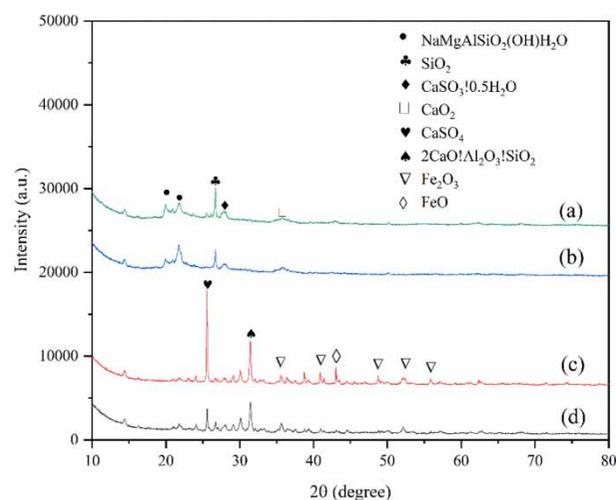
Analytical methods

Water samples were taken from batch and column studies and filtered through a 0.45 μm membrane before detection. TP, PO_4^{3-}-P, and TN were measured using an ultraviolet-

visible spectrophotometer (DR-6000, HACH, USA) according to the Chinese NEPA standard methods (NEPA 2002), and the method detection limits (MDLs) were 0.01, 0.01, and 0.05 mg/L, respectively. COD was measured through Lovibond mid-range kits with the MDL of 0–1, 500 mg/L. Furthermore, NH_4^+, Na^+, Mg^{2+}, K^+, Ca^{2+}, Cl^-, NO_2^-, NO_3^-, and SO_4^{2-} concentrations were measured using Metrohm Eco Compact IC Pro (Herisau, Switzerland) ion chromatography. The MDLs for these ions were 0.13, 0.07, 0.02, 0.07, 0,07, 0.04, 0.01, 0.01, 0.01, and 0.25 mg/L, respectively.
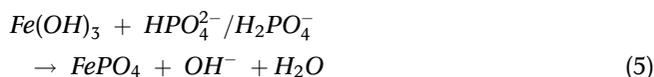
RESULTS AND DISCUSSION

XRD analysis of the adsorbents

The crystal structures of DSGA1 and DSGA2 before (fresh samples) and after (see Supplementary Information (SI)) the reaction were determined using XRD (Figure 1). There were no significant changes of peak position for both the DSGA1 and DSGA2 before and after the reaction, showing that almost no new components infiltrated to adsorbents (Hu *et al.* 2018). After the reaction, the heights of many peaks decreased significantly for DSGA2. As shown in Figure 1(c) and 1(d), it can be seen that $CaSO_4$ and Fe_2O_3 in DSGA2 that almost vanished after the reaction. Therefore, the XRD results also demonstrated that high levels of ion dissolution and chemical precipitation occurred during the removal of P using DSGA2. Barca *et al.* (2014) showed that the higher amounts of Ca and Fe in steel slag implied

a potential for P removal from polluted water. Li *et al.* (2017) suggested that fly ash was rich in Ca and Fe oxides and considered as an efficient and cheap byproduct for the adsorption of P. Kang *et al.* (2018) reported that the main elements of FGDG were Ca, O, and S. The predominant mechanisms can be postulated according to the Reaction Equations (3)–(5) (Hermassi *et al.* 2017):

$$CaO + HPO_4^{2-}/H_2PO_4^- \rightarrow CaHPO_4/Ca_5(OH)(PO_4)_3 \quad (3)$$

$$Fe_2O_3 + H_2O \rightarrow Fe(OH)_3 \quad (4)$$

$$Fe(OH)_3 + HPO_4^{2-}/H_2PO_4^- \\ \rightarrow FePO_4 + OH^- + H_2O \quad (5)$$

EPMA analysis of the adsorbents

Chemical properties of the proposed adsorbents were investigated using EPMA. White precipitation was observed in the column experiments using DSGA2. In order to further explore the adsorption mechanism, the precipitate was also collected from the Column 2# and analyzed. The results are summarized in Table 2. Considering the main elements during P adsorption, the EPMA results (Table 2) showed that DSGA1 had 2.83 Mol% of Ca as the dominant reacted mineral, followed by Fe with 0.33 Mol%. Conversely, DSGA2 had 14.42 Mol% of Ca, followed by Fe and Mg with 11.23 Mol% and 5.46 Mol%, respectively. As shown in Figure 1, it can be seen that $CaSO_4$ and Fe_2O_3 almost vanished during the reaction for DSGA2. When DSGA2 was put into the solution, the Ca^{2+} and Fe^{3+} in the material would dissolve into the KH_2PO_4 solution due to the mass transfer process. Different ionic species ($H_2PO_4^-$, HPO_4^{2-}, and PO_4^{3-}) were involved in P removal process, which

Figure 1 │ XRD patterns of (a) DSGA1 before the reaction; (b) DSGA1 after the reaction; (c) DSGA2 before the reaction; (d) DSGA2 after the reaction.

Table 2 │ Main relevant elements of the fresh and used adsorbents and the white precipitate

Element	DSGA1 Fresh (Mol%)	DSGA1 Used (Mol%)	DSGA2 Fresh (Mol%)	DSGA2 Used (Mol%)	Precipitate[a] (Mol%)
Fe	0.33	0.23	11.23	0.82	–
Ca	2.83	1.50	14.42	11.86	15.64
Mg	1.13	1.76	5.46	0.48	0.20
Al	7.39	11.43	3.91	5.77	0.30
P	0.06	0.22	0.31	0.15	5.72
Mn	–	–	2.04	1.30	–

[a]Taken from Column 2#.

were dependent on the pH of solution, as expressed by Reaction Equation (6) (Zhang *et al.* 2011). The pH values in this research were within the range 7.0–9.0, the PO_4^{3-} and HPO_4^{2-} were the main species of P. It is well known that the pK_{sp} values of $Fe_2(HPO_4)_3$ and $Ca_5(PO_4)_3OH(s)$ are 30 and 37, respectively. Hence, chemical precipitation could occur due to the ionic dissolution in this study. The results were consistent with that of XRD analysis:

$$H_3PO_4 \overset{K_1}{\to} H_2PO_4^- + H^+ \overset{K_2}{\to} HPO_4^{2-}$$
$$+ 2H^+ \overset{K_3}{\to} PO_4^{3-} + 3H^+ \tag{6}$$
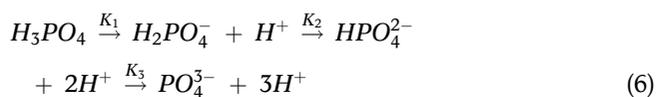
where $pK_1 = 2.15$, $pK_2 = 7.20$ and $pK_3 = 12.33$, respectively.

For DSGA1, the increase P content from 0.06 Mol% (fresh) to 0.22 Mol%. (used) may be because the surface adsorption was the main pathway for P removal. For DSGA 2, the decrease in P content from 0.31 Mol% (fresh) to 0.15 Mol% (used) may be because ion dissolution and chemical precipitation were the main pathways. The content of Mg and Al ions in DSGA1 increased from 1.13 Mol% to 1.76 Mol%, and from 7.39 Mol% to 11.43 Mol%, respectively. This could be due to the reduction of other elements, for these results represent the relative content. This can also explain the increases in the contents of Al ions from 3.91 Mol% to 5.77 Mol% in DSGA2.

According to the change in their respective contents in DSGA1 (fresh and used), the utilization efficiencies of Fe and Ca were calculated to be about 30% and 47%, respectively. As the elemental contents of Ca were higher than those of Fe, the utilization of Ca in DSGA1 was higher. This phenomenon can also be explained through the general mass transfer process. Specifically, the content of Fe in raw material was much lower than that of Ca, which led to a significant decrease in Fe content on the DSGA1 surface. As the content of Ca and Fe in DSGA2 was obviously higher than that in DSGA1, there was obvious ion dissolution and a chemical precipitation process in DSGA2. According to the change in their respective contents in DSGA2 (fresh and used), the utilization efficiencies of Fe and Ca were calculated to be about 93% and 0.18%, respectively. It is well known that the pK_{sp} values of $Fe_2(HPO_4)_3$ and $CaHPO_4$ are 30 and 7, respectively. According to the above reaction sequence, Fe^{3+} would be used first. As shown in the Supplementary information, the used DSGA2 still contained a certain amount of Ca^{2+}, so the calculated utilization rate of Ca was much lower than that of Fe in this study. Therefore, considering the utilization efficiencies mentioned above, Ca^{2+} and

Fe^{3+} were the available ions for ionic dissolution during the P removal process. It also confirmed that mixing of various industrial wastes may improve the utilization of available metal ions.

BET analysis of the adsorbents

The textural parameters of DSGA1 and DSGA2 are summarized in Table 3. As shown in Table 3, the BET surface areas of DSGA1 and DSGA2 were 17.189 and 1.721 m^2/g, respectively. The significant difference may be because DSGA1 contained 30% bentonite and 10% clay. Both bentonite and clay were clay minerals, which have smaller particle size and larger specific surface area than steel slag and fly ash. Surface areas and the pore size distributions of the adsorbents were the main influencing factors of physical adsorption (Li *et al.* 2016). Combined with the changes in P content in adsorbents (fresh and used) (shown in Table 2), surface adsorption and chemical precipitation may be the main pathways for DSGA1 and DSGA2, respectively.

SEM analysis of the adsorbents

The SEM images for DSGA1 and DSGA2 before and after reaction are shown in Figure 2. Figure 2(a)–2(d) shows that DSGA1 and DSGA2 had rough surfaces and many small holes were observed on their surfaces and the internal structure. Therefore, surface and internal diffusion could occur in P removal. As shown in Figure 2(e)–2(h), many floccules were present during the experiments for both DSGA1 and DSGA2. Figure 2(g) and 2(h) show that the internal pores became markedly larger and shallower for DSGA2. This suggests that many ions may dissociate from DSGA2 and a new surface would be formed, finally. Then, the dissolved ions would incur further chemical precipitation in solution. These results were consistent with the results observed by XRD and EPMA. First, XRD results showed that $CaSO_4$ and Fe_2O_3 in DSGA2 almost vanished after the reaction (Figure 1(c) and 1(d)). Second, EPMA results showed that the main elements in white precipitation were Ca and P (Table 2). The appearance of floccules may be

Table 3 | BET results of DSGA1 and DSGA2

Type of material	BET surface area (m²/g)	Total pore volume (cm³/g)	Average pore diameter (nm)
DSGA1	17.189	0.116	4.911
DSGA2	1.721	0.003	1.446
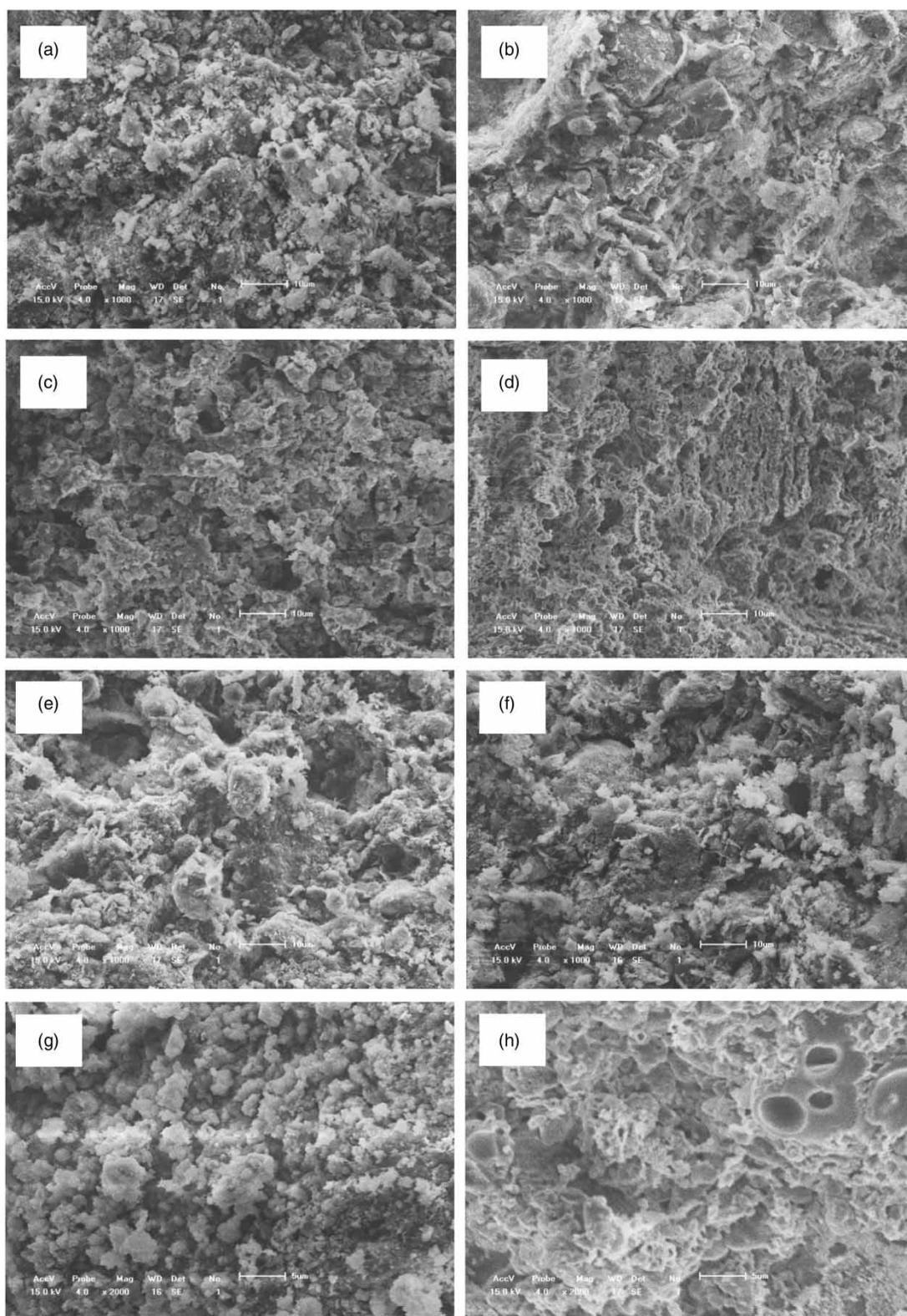
Figure 2 │ Scanning electron microscope (SEM) images: (a) Surface of DSGA1 before the reaction; (b) interior of DSGA1 before the reaction; (c) surface of DSGA2 before the reaction; (d) interior of DSGA2 before the reaction; (e) surface of DSGA1 after the reaction; (f) interior of DSGA1 after the reaction; (g) surface of DSGA2 after the reaction, and (h) interior of DSGA2 after the reaction.

due to the adsorption of precipitates or/and P on the surface.

Effect of contact time on adsorption capacity

The contact time of adsorbent and solution had a great significance in practical applications. When the adsorption reached equilibrium in the batch experiments, there is maximum contact time. Generally, this can provide reference for hydraulic retention time. The results for the adsorption capacities of DSGA1 and DSGA2 are illustrated in Figure 3. The removal capacity of DSGA1 and DSGA2 reached the maximum at 96 and 312 h, respectively. However, the maximum adsorption capacity for DSGA2 was 15.85 mg P/g, which was 19 times higher than that of DSGA1 (0.82 mg P/g).

During the first 24 h, the adsorption capacity of DSGA2 increased over time and the rate was 0.065 mg $g^{-1} h^{-1}$ ($R^2 = 0.959$). Between 24 and 48 h, the adsorption rate decreased, which was similar to the previously reported results (Chen *et al.* 2012). As reported in a previous study, the reaction would reach equilibrium according to the trend analysis of 24–48 h, whereas the tendency for equilibrium would be indicated by the results presented in Figure 3 in black dotted lines. However, adsorption rate was 0.035 mg $g^{-1} h^{-1}$ ($R^2 = 0.997$) between 48 and 144 h, highlighting a strong increasing trend compared to the black dotted lines. This could be due to the ionic dissolution between 48 and 144 h of the adsorption process. During 144–264 h, the rate was 0.073 mg $g^{-1} h^{-1}$ ($R^2 = 0.998$), which was similar to the value at 0–24 h. Hence, a new

surface may have formed at 144 h. In the final stage (>264 h), the rate decreased over time and became almost zero. Therefore, in this research, it can be inferred that there were three distinct pathways (shown in Figure 4) for P removal using DSGA2, which included surface adsorption, internal diffusion, and ionic dissolution. These results were in line with previous studies (Gu *et al.* 2021).

Therefore, the P removal mechanisms for both DSGA1 and DSGA2 include three pathways, in which surface adsorption and chemical precipitation were the main pathways for DSGA1 and DSGA2, respectively. The possible adsorption pathways for P removal are shown in Figure 4.

There are two reasons for the different adsorption capacities between DSGA1 and DSGA2. On the one hand, the contents of metal ions in DSGA2 were relatively higher than DSGA1 due to the presence of steel slag and fly ash. Some previous studies have reported that steel slag and fly ash were effective P removal materials and rich in minerals (Claveaumallet *et al.* 2013). The EPMA results (Table 2) showed that the contents of Fe and Ca in DSGA2 were 34 times and five times that in DSGA1. On the other hand, fly ash, and steel slag may improve the utilization of available metal ions in FGDG. Synergistic effects might exist among various kinds of industrial wastes used to synthesize DSGA2. The utilization efficiencies of Fe in DSGA1 and DSGA2 were calculated to be about 30% and 93%, respectively. Cheng *et al.* (2018) reported that, for the nanosized desulfurization gypsum, the maximum adsorption capacity was 23.66 mg P/g ($R^2 = 0.999$). The adsorption capacity of granular adsorbent of DSGA2 was 15.85 mg P/g, which was close to the maximum release of
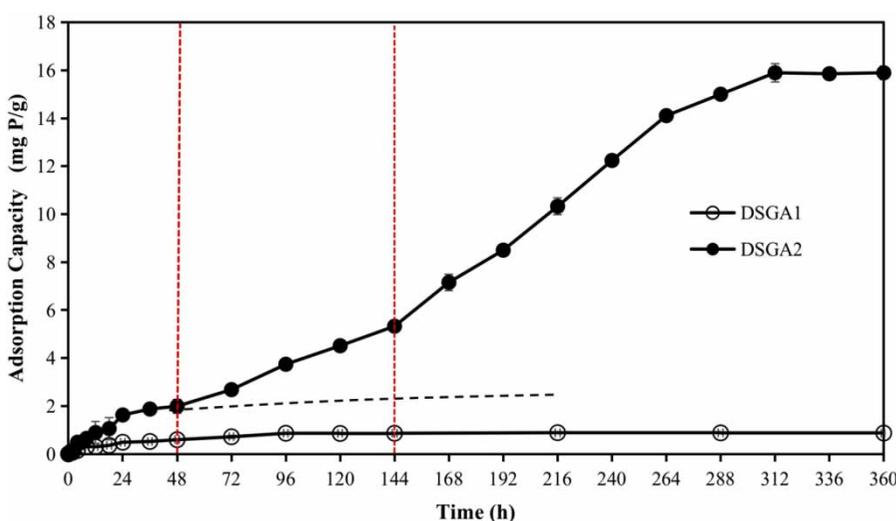

Figure 3 │ Relationship between the contact times and adsorption capacities of DSGA1 and DSGA2.
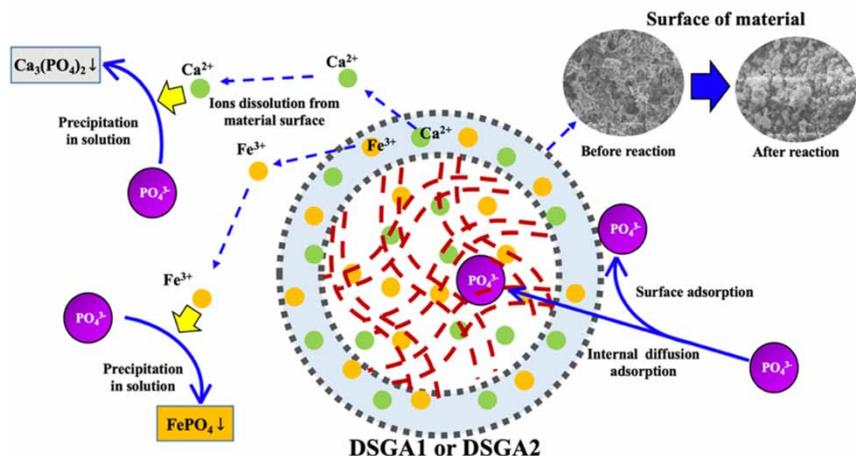
Figure 4 | P adsorption mechanisms for DSGA1 and DSGA2.

nanoscale. The result also verified that the existence of steel slag and fly ash improves the utilization ratio of FGDG. Therefore, mixing various kinds of industrial wastes has been proven as a cost-effective method to improve the utilization of these waste materials and their adsorption capacity for P.

In addition, DSGA2 contained about 2.04 Mol% Mn (Table 2). The element Mn concentration in solution was kept lower than the MDL of 0.005 mg/L during the process, which may be because DSGA2 was only composed of 20% steel slag and Mn was fixed on it without dissolution. Hydroxyapatite was reported as a highly effective heavy metal adsorbent with low water solubility and high stability (Meski *et al.* 2010). This may be further reducing the risk of

heavy metal contamination when chemical precipitation occurs and hydroxyapatite was formed in the process of P removal.

Estimation of the breakthrough curves

Breakthrough curves for two kinds of influent waters are presented in Figure 5. In Column 1#, over 92% of P removal was achieved in 5 d after the operation, whereas the Q_p value was 2.50 mg/g. The first value greater than 10% (breakthrough point) for Column 1# was 0.12 (12%) at 5.5 d. It was at 8.0 d that the first point greater than 10% (14%) appeared in Column 2#, which then disappeared in the next sample. Both the columns were subjected to interruption tests
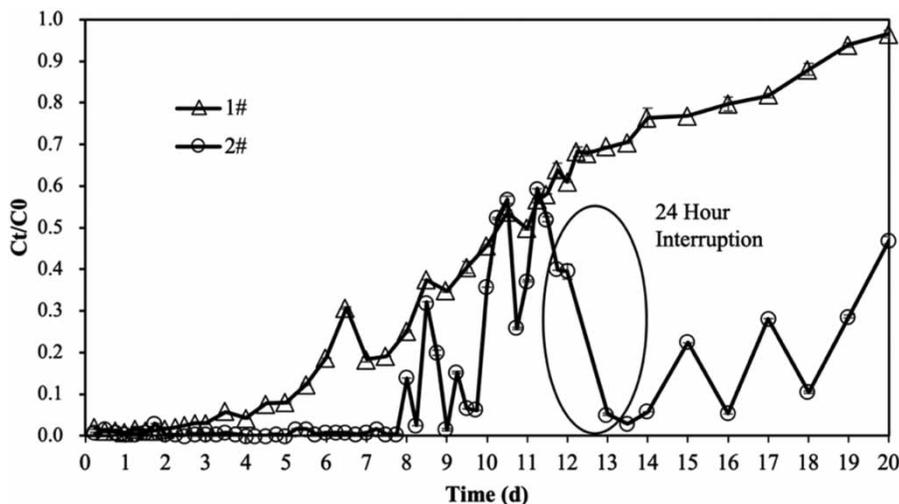

Figure 5 | Breakthrough curves of Columns 1# (influent was the actual SWW) and 2# (influent was the synthetic P-contained solution) showing interruption tests. (Note that C_0 is the initial P concentration, C_t is the P concentration at time t.)

during the periods of 12 d. The corresponding results are marked in circles in Figure 5. After the 24 h interruption, it can be seen that only the treatment effect of Column 2# was restored. This illustrated that Column 2# was easier to be regenerated than Column 1# during the process.

No suitable typical breakthrough curves were found for use in Columns 1# and 2#. On the one hand, it was apparent that a fraction of adsorption sites was not easily accessible. Therefore, the effluent P concentration became unstable during the process. On the other hand, the complex internal structure and pores of the particles were used to explain this phenomenon (Ouvrard *et al.* 2002). Furthermore, a better treatment effect was observed immediately after the interruption in Column 2#. It may testify that the mass transfer process, especially the intraparticle diffusion, played a significant role when column was fed with KH_2PO_4 solution (Demarco *et al.* 2003; Greenleaf & Sengupta 2006; Sengupta & Pandit 2011). It also validated the above presumption that P removal using DSGA2 included surface adsorption, internal diffusion, and ionic dissolution. This can successfully explain why only Column 2# was regenerated after the 24 h interruption. This was because the presence of various ions in the actual SWW can affect the P intraparticle diffusion process.

Effect of the co-existing anions

The SWW contained various kinds of co-existing anions, which could potentially compete with P for the adsorptive sites (He *et al.* 2016), thus accordingly affecting the performance of P removal. The effects of typical co-existing cations and anions, such as NH_4^+, Mg^{2+}, K^+, Na^+, NO_2^-, NO_3^-, and Cl^- on the adsorption process were investigated. The concentrations of cations and anions in SWW were found in the following descending order: $Na^+ > K^+ > Mg^{2+} > NH_4^+$ [Figure 6(a)] and $NO_3^- > Cl^- > NO_2^-$ [Figure 6(b)]. Figure 6(c) and 6(d) demonstrate the cations that mainly consisted of Ca^{2+} and K^+, whereas the anions were SO_4^{2-} in Column 2#.

Comparing Figure 6(a) and 6(c), there were consistent trends for Ca^{2+} in the two columns although the concentrations of the cation were different. These results showed that Ca^{2+} was the major cation reacting with P [Figure 6(a) and 6(c)]. Moreover, there was white precipitation in both the columns. In order to minimize the disruption caused by other factors, the precipitate was collected from Column 2#. The elemental results of white precipitation are also presented in Table 2. As shown by the results presented in Table 2, the precipitate had 15.64 Mol% of Ca
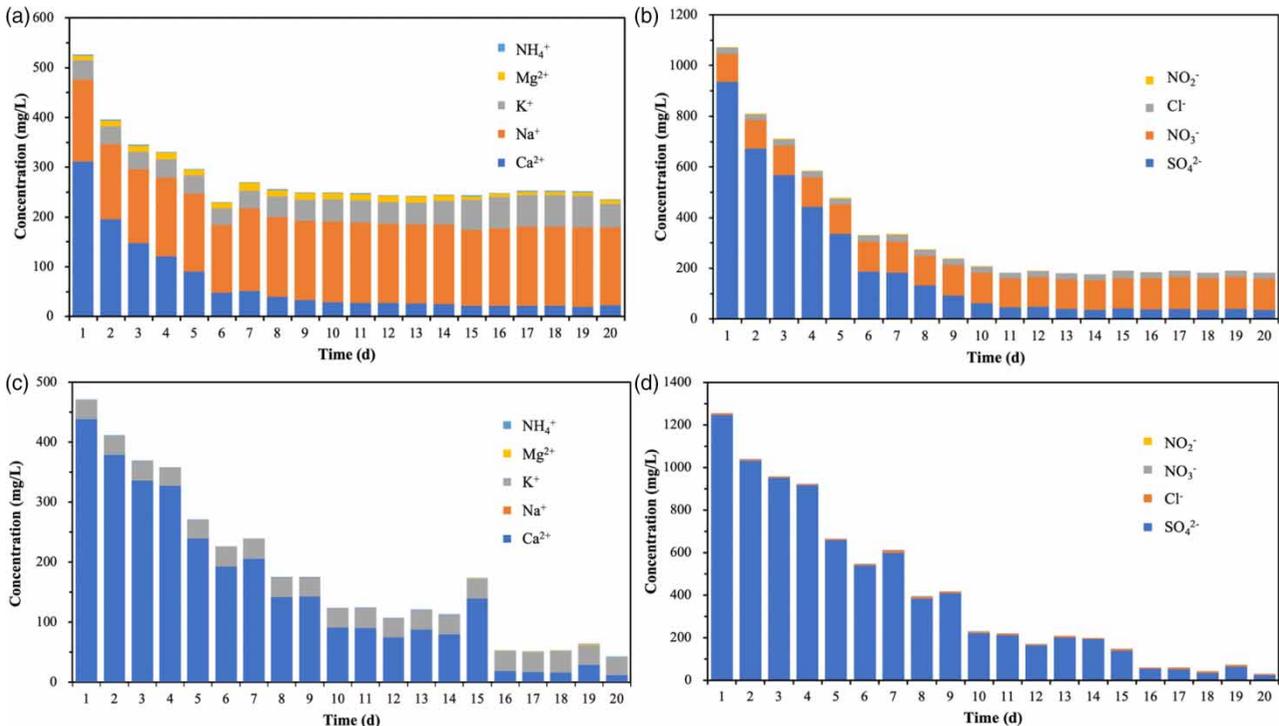

Figure 6 | Temporal changes in cation and anion concentrations in the reactors: (a) Cation of Column 1#; (b) Anion of Column 1#; (c) Cation of Column 2# and (d) Anion of Column 2#.

and 5.72 Mol% of P, whereas no Fe was detected. Given that the pH values of Column 1# effluent were within the range of 7.0–9.0, Fe reacted with P first, Fe-P precipitates was formed firstly in the reaction. However, the column experiment lasted for 20 days, which made the Fe-P precipitate discharge with the effluent, and the final precipitate was mainly Ca-P precipitate. The adsorbent itself has a high calcium content, which leads to the relatively low iron content in the final precipitate and, consequently, not detected in the precipitate.

Comparing Figure 6(b) and 6(d), it can be seen that the SO_4^{2-} concentration in Column 1# was lower than that in Column 2#. This could be because the presence of various anions in the actual SWW not only interrupted the intraparticle diffusion, but slowed down the dissolution of $CaSO_4$. Therefore, the whole P removal process of the Column 1# remained more or less stable. There were many kinds of ions in SWW, but the NO_3^- concentration in the secondary SWW effluent was the largest one. Hence, the difference between the two columns should be due to the exist of high NO_3^-, which may inhibit PO_4^{3-} removal performance. It is worth noting that there were different C_t/C_o variation trends between Columns 1# and 2# with the decrease in the Ca^{2+} and SO_4^{2-} concentrations. The C_t/C_o of Column 1# increased, while that of Column 2# had even lower values. Therefore, as the amounts of Ca and Fe in DSGA2 gradually decreased, it still had a certain adsorption capacity. This capacity may be due to the surface adsorption and intraparticle diffusion process. This phenomenon accords with our conjecture about the three pathways for the adsorption process. All of these results were crucial for the practical application of DSGA2.

Engineering significance

This study demonstrated that DSGA2 can be used as an efficient and low-cost adsorbent to remove P from SWW and achieve the idea of controlling waste by using waste in practical engineering applications. The characteristics of meat processing wastewater were similar to that of SWW. Due to the lower contamination of meat processing wastewater, DSGA2 was also feasible for industrial application in the meat sector as future application. Further studies should be conducted to study this hypothesis. According to the results and analysis conducted in the current work, the developed industrial wastes-based adsorbents have a good economical and environmental benefit, and should be popularized.

CONCLUSIONS

Mixing various kinds of industrial wastes is a cost-effective modification method for improving the adsorption capacity of adsorbents due to the availability of various metal ions. The maximum adsorption capacity for DSGA2 composed of 60% FGDG, 20% steel slag, and 20% fly ash was 15.85 mg P/g. The column experiments showed that the Q_p value of 2.50 mg P/g highlighted the potential of DSGA2 to be used in actual engineering applications. DSGA2 presented more stable P removal when fed with actual secondary SWW effluent than the synthetic P-containing wastewater. Therefore, the synthesized DSGA2 showed a broader application prospect due to its low-cost in wastewater treatment and the reuse of industrial wastes. It showed the potential for application in practical projects to replace the traditional chemical precipitation methods used for adsorbing various pollutants.

CONFLICTS OF INTEREST

The authors declare no conflict of interest.

ACKNOWLEDGEMENTS

DATA AVAILABILITY STATEMENT

All relevant data are included in the paper or its Supplementary Information.

REFERENCES

Barca, C., Meyer, D., Liira, M., Drissen, P., Comeau, Y., Andrès, Y. & Chazarenc, F. 2014 Steel slag filters to upgrade phosphorus removal in small wastewater treatment plants: removal mechanisms and performance. *Ecol. Eng.* **68**, 214–222.

Bouwman, L., Goldewijk, K. K. & Van, D. H. K. W. 2013 Exploring global changes in nitrogen and phosphorus cycles in agriculture induced by livestock production over the 1900–2050 period. *Proc. Natl. Acad. Sci. USA* **110** (52), 20882–20887.

Chen, N., Feng, C., Zhang, Z., Liu, R., Gao, Y., Li, M. & Sugiura, N. 2012 Preparation and characterization of lanthanum (III) loaded granular ceramic for phosphorus adsorption from aqueous solution. *J. Taiwan Inst. Chem. Eng.* **43** (5), 783–789.

Chen, D., Szostak, P., Wei, Z. & Xiao, R. 2016 Reduction of orthophosphates loss in agricultural soil by nano calcium sulfate. *Sci. Total Environ.* **539**, 381–287.

Cheng, P., Chen, D. & Liu, H. 2018 Synergetic effects of anhydrite and brucite-periclase materials on phosphate removal from aqueous solution. *J. Mol. Liq.* **254**, 145–153.

Claveaumallet, D., Wallace, S. & Comeau, Y. 2013 Removal of phosphorus, fluoride and metals from a gypsum mining leachate using steel slag filters. *Water Res.* **47** (4), 1512–1520.

Demarco, M. J., Sengupta, A. K. & Greenleaf, J. E. 2003 Arsenic removal using a polymeric/inorganic hybrid sorbent. *Water Res.* **37** (1), 164–176.

Greenleaf, J. E. & Sengupta, A. K. 2006 Environmentally benign hardness removal using ion-exchange fibers and snowmelt. *Environ. Sci. Technol.* **40** (1), 370–376.

Gu, S., Fu, B., Ahn, J. W. & Fang, B. 2021 Mechanism for phosphorus removal from wastewater with fly ash of municipal solid waste incineration, Seoul, Korea. *J. Cleaner Prod.* **280**, 124430.

He, Y., Lin, H., Dong, Y., Liu, Q. & Wang, L. 2016 Simultaneous removal of phosphate and ammonium using salt-thermal-activated and lanthanum-doped zeolite: fixed-bed column and mechanism study. *Desalin. Water Treat.* **57** (56), 27279–27293.

Hermassi, M., Valderrama, C., Moreno, N., Font, O., Querol, X., Batis, N. H. & Cortina, J. L. 2017 Fly ash as reactive sorbent for phosphate removal from treated wastewater as a potential slow release fertilizer. *Environ. Chem. Eng.* **5**, 160–169.

Hu, F., Wang, M., Peng, X., Qiu, F., Zhang, T., Dai, H., Liu, Z. & Cao, Z. 2018 High-efficient adsorption of phosphates from water by hierarchical CuAl/biomass carbon fiber layered double hydroxide. *Colloids Surf. A.* **555**, 314–323.

Kang, J., Gou, X., Hu, Y., Sun, W., Liu, R., Gao, Z. & Guan, Q. 2018 Efficient utilisation of flue gas desulfurization gypsum as a potential material for fluoride removal. *Sci. Total Environ.* **649**, 344–352.

Li, M., Liu, J., Xu, Y. & Qian, G. 2016 Phosphate adsorption on metal oxides and metal hydroxides: a comparative review. *Environ. Rev.* **24** (3), 319–332.

Li, S., Cooke, R. A., Wang, L., Ma, F. & Bhattarai, R. 2017 Characterization of fly ash ceramicpellet for phosphorus removal. *J. Environ. Manage.* **189**, 67–74.

Meski, S., Ziani, S. & Khireddine, H. 2010 Removal of lead ions by hydroxyapatite prepared from the egg shell. *J. Chem. Eng. Data* **55** (9), 3923–3928.

NEPA 2002 *Water and Wastewater Monitoring Analysis Method*, 4th edn. China Environmental Science Press, Beijing. (in Chinese)

Nguyen, T. A. H., Ngo, H. H., Guo, W. S., Zhang, J., Liang, S., Lee, D. J., Nguyen, P. D. & Bui, X. T. 2014 Modification of agricultural waste/by-products for enhanced phosphate removal and recovery: potential and obstacles. *Bioresour. Technol.* **169**, 750–762.

Ouvrard, S., Simonnot, M. O. & De Donato, P. 2002 Diffusion-controlled adsorption of arsenate on a natural manganese oxide. *Ind. Eng. Chem. Res.* **41** (24), 6194–6199.

Prazeres, A. R., Fernandes, F., Madeira, L., Silvana, L., Albuquerque, A., Simões, R., Beltrán, F., Jerónimo, E. & Rivas, J. 2019 Treatment of slaughterhouse wastewater by acid precipitation (H_2SO_4, HCl and HNO_3) and oxidation (Ca(ClO), H_2O_2 and CaO). *J. Environ. Manage.* **250**, 109558.

Sengupta, S. & Pandit, A. 2011 Selective removal of phosphorus from wastewater combined with its recovery as a solid-phase fertilizer. *Water Res.* **45** (11), 3318–3330.

Tong, S., Wang, S., Zhao, Y., Feng, C., Xu, B. & Zhu, M. 2019 Enhanced alure-type biological system (E-ATBS) for carbon, nitrogen and phosphorus removal from slaughterhouse wastewater: a case study. *Bioresour. Technol.* **274**, 244–251.

Xue, Y., Hou, H. & Zhu, S. 2009 Adsorption removal of reactive dyes from aqueous solution by modified basic oxygen furnace slag: isotherm and kinetic study. *Chem. Eng. J.* **147** (2-3), 272–279.

Yin, Y., Xu, G., Li, L., Xu, Y., Zhang, Y., Liu, C. & Zhang, Z. 2020 Fabrication of ceramsite adsorbent from industrial wastes for the removal of phosphorus from aqueous solutions. *J. Chem.* **2020**, 1–13.

Zhang, J., Shen, Z., Shan, W., Mei, Z. & Wang, W. 2011 Adsorption behavior of phosphate on lanthanum (III)-coordinated diamino-functionalized 3D hybrid mesoporous silicates material. *J. Hazard. Mater.* **186** (1), 76–83.